UPPSALA
UNIVERSITET

UPTEC IT 12 015
Examensarbete 30 hp
September 2012

Evaluating the accuracy of motion tracking algorithms for determining the position of finger tips

Malin Nilsson

UPPSALA
UNIVERSITET

Teknisk- naturvetenskaplig fakultet
UTH-enheten

Besöksadress:
Ångströmlaboratoriet
Lägerhyddsvägen 1
Hus 4, Plan 0

Postadress:
Box 536
751 21 Uppsala

Telefon:
018 – 471 30 03

Telefax:
018 – 471 30 00

Hemsida:
http://www.teknat.uu.se/student

Abstract

Evaluating the accuracy of motion tracking algorithms for determining the position of finger tips

Malin Nilsson

Motion capture, or motion tracking, describes the process of recording movement of objects. Motion capture for biomechanical applications often involves sensors or markers that are placed on the skin of body segments. The position of these markers is measured as the subject moves. In this thesis, motion capture is used to record movements of the hand and fingers. Two methods for estimation of sensor positions, Method A and Method B, are investigated. These methods are based on kinematic models describing the studied system, where states are estimated with an Extended Kalman Filter. In many applications it is important to estimate the position of the finger tips accurately, but it is not always possible to place sensors on them. Therefore the methods are first modified to also estimate the positions of the finger tips based on the estimated positions of the markers. Then, the accuracy of the methods are evaluated in terms of a specific accuracy measure, for different values of the user parameters of the methods. The effect of the user parameters is investigated and appropriate values for them, i.e values that give the best performance, are given. It is shown that Method B performs better than Method A and that it also is less sensitive to the choice of user parameters, but Method A could be considered easier to use and easier to apply to general kinematic systems.

Handledare: Kjartan Halvorsen
Ämnesgranskare: Håkan Lanshammar
Examinator: Arnold Pears
ISSN: 1401-5749, UPTEC IT12 015
Tryckt av: ITC

Sammanfattning

Motion Capture, eller Motion Tracking, går ut på att mäta och spela in hur olika objekt rör sig. I biomekaniska tillämpningar av Motion Capture används ofta sensorer, eller markörer, som fästs på huden på olika kroppsdelar hos en försöksperson. Man mäter sedan markörernas position, medan personen rör sig. I det här arbetet används Motion Capture för att spela in handens och fingrarnas rörelser då fingerspetsarna rör sig över en plan platta. Mätdata som man får från sensorerna är brusiga och är därför inte alltid tillräckligt bra för användning i vissa tillämpningar. För att minska bruset kan man använda sig av metoder som brusreducerar med hjälp av kinematiska modeller av det studerade systemet. Två sådana metoder undersökes i detta arbete. I modellerna finns variabler som beskriver olika vinklar och avstånd i systemet. Dessa variabler ändras med tiden och kan skattas med hjälp av ett så kallat Extended Kalman Filter (EKF). När alla vinklar och avstånd är kända kan förfinade versioner av sensormätningarna tas fram.

I många applikationer är det viktigt att bestämma fingerspetsarnas position noggrannt, men det är inte alltid möjligt att sätta sensorer på dem. Metoderna modifieras därför först för att kunna bestämma fingerspetsarnas position utifrån de skattade markörpositionerna. I båda metoderna finns ett antal parametrar som måste ställas in av användaren. Dessa parametrar påverkar metodernas noggrannhet. Vilka värden som fungerar bäst beror på systemet man studerar och det mätdata man samlat in. Effekten av användarparametrarna på metodens noggrannhet undersöks och lämpliga värden, dvs värden som ger bäst prestation, på parametrarna ges. Det visar sig att Metod B presterar bättre än Metod A, och att den också är mindre känslig för valet av användarparametrar, men Metod A kan ses som lättare att använda och lättare att applicera på generella kinematiska system.

Contents

Chapter 1

Introduction

Motion capture, or motion tracking, describes the process of recording movement of objects. It is used in military, entertainment, sports, medical applications and more [1]. Motion capture for biomechanical applications often involves sensors or markers that are placed on the skin of body segments. The position of these markers is measured as the subject moves. The collected data can then be used to reconstruct the motion of the body part. The system described in [2] is designed for interacting with 3D, virtual and dynamic objects rendered by a holographic display. The system includes a haptic glove which makes you experience that you are grabbing an actual physical object. One application for this is in jaw surgery, where the surgeon could use this technique to practice difficult operations without running the risk of injuring a patient. Motion capture is an important element of this. If the haptic glove is to work as expected, the positions of the tips of the fingers have to be known. The measured data from the markers is noisy, which could be a problem, therefore it may be important to use motion capture models to filter the data to remove the noise.

The purpose of this project is to modify two existing motion capture model implementations, and then to investigate and compare the accuracy of the two methods for estimating the position of the tips of the fingers from motion capture data. The implementations must first be modified to only describe the hand and finger movements, and then equations must be added

to calculate the coordinates of the finger tips. The tracking algorithms and their ability to reconstruct the finger positions from measured data must then be evaluated. Specifically, the precision of the algorithms when estimating the finger tip positions as they move over a known surface must be established. Therefore an appropriate accuracy measure must be chosen and applied. More specifically, the goals are:

- To find out which is the better method.
- To establish whether any of the methods improve the results compared to using measured data directly.
- To determine how important the choice of the user parameters are in the two methods.

The reason for doing this is to simplify future studies of virtual object interaction by providing a reliable estimation method. The first of the two implementations that will be modified is a toolbox by Todorov (2007) [3] that contains a framework for constructing kinematic models of general segments and joint structures. The second was derived by Halvorsen et al. (2008) [4]. It estimates the movement of the forearm, the palm and all five fingers. These two methods will be adapted to model the forearm, the hand, the index finger and the middle finger.

Chapter 2

Method

2.1 Modelling

In this study we choose to model only the forearm, the hand and two fingers. The forearm and hand can be described by a number of segments connected by joints. The hand is one segment, the forearm is one segment and each finger consist of three segments. One sensor was placed on each finger segment; the distal phalange, the intermediate phalange and the proximal phalange. Two were placed on the palm of the hand, and three sensors were placed on the forearm. All sensors were placed on the skin except for the one on the distant phalange which was placed on the nail. Two approaches were used to model this and to estimate the model states, one by Todorov and one by Halvorsen et al. The method derived by Todorov will be referred to as Method A and the one based on the model by Halvorsen et al. will be referred to as Method B.

2.1.1 Method A

Todorov has developed a toolbox for movement estimation and self-calibration from motion capture data, and we will use this toolbox to create a model for the forearm and hand and estimate its states. Using the toolbox involves three steps.

1. Constructing a kinematic model specifying how the sensor measure-

ments depend on the state vector. The model also requires specification of the process noise covariance matrix R.

2. Collecting motion-capture data compatible with the model created in step 1.

3. Applying the estimation algorithm. Initial values for the state vector and the state covariance matrix are required.

In each time step the model decides a maximum aposteriori estimation of the state vector by using an iterative algorithm. If only one iteration is carried out the algorithm is an extended Kalman filter.

Before this toolbox could be used, the system, i.e. all the joints and how they are connected, had to be described in detail. The kinematic model could then be described as an Nx5 matrix where N is the number of segments. The integers in the matrix decide the properties of the model. To give more clarity this model has, with the help of the matrix, been drawn as a tree shown in figure 2.1. In this tree the segments can correspond to limb segments, dummy segments or sensors, which are all connected by joints. Rectangles represent segments/frames and circles represent joints/transformations. Shaded circles correspond to constant transformations while empty circles corresponds to time-varying transformations. Rectangles with heavy outlines represent frames whose position are being measured by sensors. Two segments can only be connected with a single joint, so if there is both a translation and a rotation of the same joint a dummy segment needs to be placed between the two joints.

The four different joint types are the following:

	Joint type	**Description**	**Degrees of freedom**
1	S(liding)	Translation in predefined direction	1
2	T(ranslation)	Translation in any direction	3
3	H(inge)	Rotation around predefined axis	1
4	R(otation)	Rotation around any axis	3

1. Sliding joints have one parameter specifying the sliding distance.

2. Translation joints have three parameters, which specify the translation vector.

3. Hinge joints have one parameter, specifying the rotation angle.

4. Rotation joints have three parameters, specifying an angle-axis vector. The length of this vector is the rotation angle, and the direction of the vector is the rotation axis.

The states of this model are the free parameters of each joint. Since joints can be set as fixed, constant but unknown parameters, such as limb lengths, can be estimated using this model. The kinematic tree can be represented as a table, which contains all information about the segments and their connecting joints. Fig. 2.1 is represented in tabular form in table 2.1. The state equations are given by

$$x_j(k+1) = x_j(k) + u_j(k) \tag{2.1}$$

where x_j is the j:th state variable and $u_j(k)$ is white noise with variance σ_j^2, the process noise. For states representing constant parameters, σ_j^2 is set to 0. This means that the state estimator will assume that these states do not change in time. The output from the model is given by

$$\mathbf{y}(k) = f(\mathbf{x}) + \mu(k) \tag{2.2}$$

where $\mathbf{y}$ contains the coordinates for all sensors, f is the nonlinear function describing how the markers depend on the states and $\mu(k)$ is white measurement noise with

$$E[\mu(k)\mu^T(k)] = \mathbf{R}_\mu(k). \tag{2.3}$$

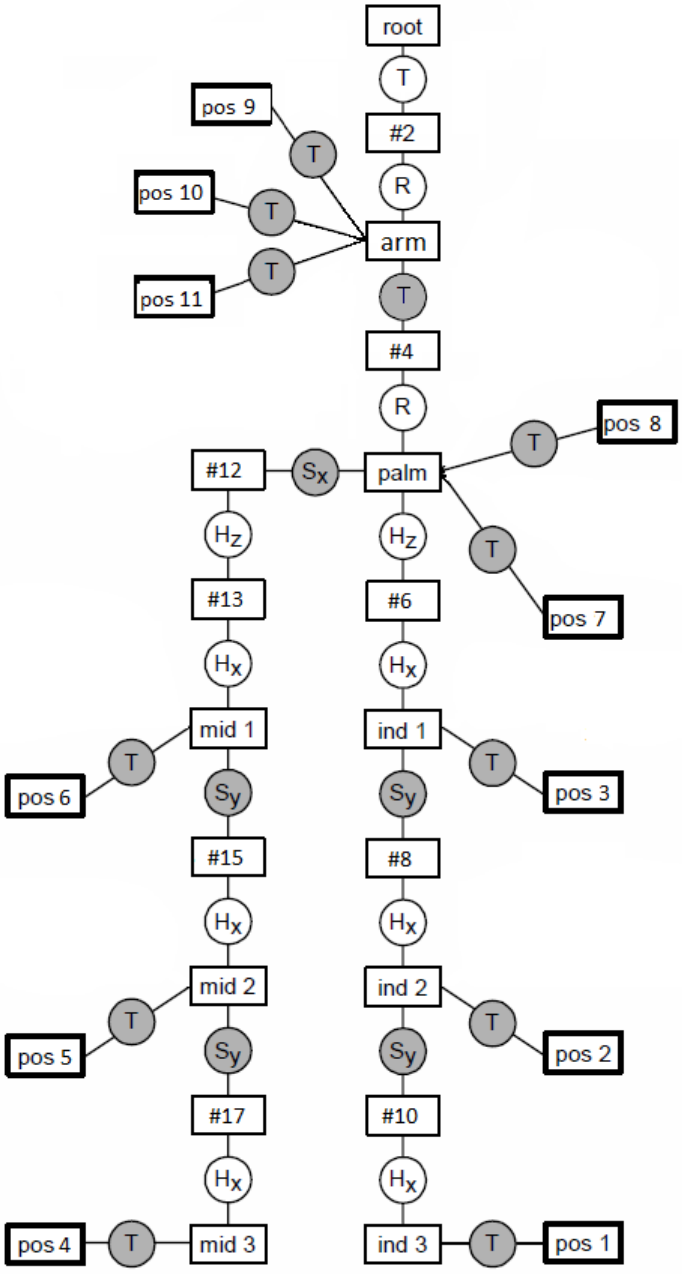

Figure 2.1: The tree describing the kinematic model.

Segment name (#)	**Parent segment**	**Joint type**	**Sensor type**	**Joint axis**	**Joint category**
root(1)	none	none(0)	none(0)	none(0)	none(0)
dummy(2)	root(1)	translate(2)	none(0)	none(0)	varying(1)
arm(3)	dummy(2)	rotate(4)	none(0)	none(0)	varying(1)
dummy(4)	arm(3)	translate(2)	none(0)	none(0)	constant(2)
palm(5)	dummy(4)	rotate(4)	none(0)	none(0)	varying(1)
dummy(6)	palm(5)	hinge(3)	none(0)	z(3)	varying(1)
ind1(7)	dummy(6)	hinge(3)	none(0)	x(1)	varying(1)
dummy(8)	ind1(7)	slide(1)	none(0)	y(2)	constant(2)
ind2(9)	dummy(8)	hinge(3)	none(0)	x(1)	varying(1)
dummy(10)	ind2(9)	slide(1)	none(0)	y(2)	constant(2)
ind3(11)	dummy(10)	hinge(3)	none(0)	x(1)	varying(1)
dummy(12)	palm(5)	slide(1)	none(0)	x(1)	constant(2)
dummy(13)	dummy(12)	hinge(3)	none(0)	z(3)	varying(1)
mid1(14)	dummy(13)	hinge(3)	none(0)	x(1)	varying(1)
dummy(15)	mid1(14)	slide(1)	none(0)	y(2)	constant(2)
mid2(16)	dummy(15)	hinge(3)	none(0)	x(1)	varying(1)
dummy(17)	mid2(16)	slide(1)	none(0)	y(2)	constant(2)
mid3(18)	dummy(17)	hinge(3)	none(0)	x(1)	varying(1)
pos1(19)	ind3(11)	translate(2)	pos(2)	none(0)	constant(2)
pos2(20)	ind2(9)	translate(2)	pos(2)	none(0)	constant(2)
pos3(21)	ind1(7)	translate(2)	pos(2)	none(0)	constant(2)
pos4(22)	mid3(18)	translate(2)	pos(2)	none(0)	constant(2)
pos5(23)	mid2(16)	translate(2)	pos(2)	none(0)	constant(2)
pos6(24)	mid1(14)	translate(2)	pos(2)	none(0)	constant(2)
pos7(25)	palm(5)	translate(2)	pos(2)	none(0)	constant(2)
pos8(26)	palm(5)	translate(2)	pos(2)	none(0)	constant(2)
pos9(27)	arm(3)	translate(2)	pos(2)	none(0)	constant(2)
pos10(28)	arm(3)	translate(2)	pos(2)	none(0)	constant(2)
pos11(29)	arm(3)	translate(2)	pos(2)	none(0)	constant(2)

Table 2.1: The segment matrix describing the kinematic model.

2.1.2 Method B

The model derived by Halvorsen et al. is presented in [4]. It is a dynamic model on state space form, where the states are the angles and their angular velocities and the output signal is the markers' position coordinates. The angular velocities are modelled as random walks and the angles as the integral of the velocities. The output signal is written as a function of the states by means of rotation matrices. This function is nonlinear so a standard Kalman filter can not be used to estimate the states. Instead, an extended Kalman filter (EKF) is used.

The model equations can be derived as follows: Let $\phi(t)$ be the joint angles in the model. The assumption in the model is that each angular acceleration is white noise, i.e

$$\ddot{\phi}(k) = \mathbf{w}(k) \tag{2.4}$$

where $\mathbf{w}(k)$ is white noise with the covariance matrix

$$E[\mathbf{w}(k)\mathbf{w}^T(k+\tau)] = \mathbf{R}_w\delta(\tau) \tag{2.5}$$

where $\delta(\tau)$ is Dirac's δ function and $\mathbf{R}_w$ is a diagonal matrix. Let $\mathbf{x}(k)$ be the state vector in the model. The first half of the vector consists of the angles $\phi(k)$ and the second half consists of their angular velocities $\dot{\phi}(k)$. It is shown in [4] that the state equations for $\mathbf{x}(k)$ then becomes

$$\mathbf{x}(k+1) = F\mathbf{x}(k) + \mathbf{v}(k) = \begin{bmatrix} \mathbf{I} & h\mathbf{I} \\ 0 & \mathbf{I} \end{bmatrix} \mathbf{x}(k) + \mathbf{v}(k) \tag{2.6}$$

where $\mathbf{I}$ is the identity matrix and h is the sampling period. The covariance matrix of the process noise $\mathbf{v}(k)$ has the form

$$E[\mathbf{v}(k)\mathbf{v}^T(k)] = \begin{bmatrix} (1/3)h^3\mathbf{R}_w(k) & (1/2)h^2\mathbf{R}_w(k) \\ (1/2)h^2\mathbf{R}_w(k) & h\mathbf{R}_w(k) \end{bmatrix}. \tag{2.7}$$

The output from the model is given by

$$\mathbf{y}(k) = vect(\begin{bmatrix} \mathbf{G}^{(1)}(k)\mathbf{p}_0^{(1)} \dots \mathbf{G}^{(L)}(k)\mathbf{p}_0^{(L)} \end{bmatrix}) + \mathbf{e}(k) \tag{2.8}$$

where $\mathbf{p}_0^{(i)}$ contains the coordinates for all markers on segment i when the system is in its reference position, and the matrices $\mathbf{G}^{(i)}(k)$ are functions of $\phi(k)$ describing the rotation of each segment. $\mathbf{p}_0^{(i)}(k)$ are matrices where each column contains the coordinates for one marker, the vect-function stacks these columns in one single vector. $\mathbf{e}(k)$ is white noise with

$$E[\mathbf{e}(k)\mathbf{e}^T(k)] = \mathbf{R}_\mathbf{e}(k). \tag{2.9}$$

The behavior of the EKF will depend on how $\mathbf{R}_w$ in (2.5) and $\mathbf{R}_e$ in (2.9) are chosen.

The model in [4] includes five fingers, the hand and the arm. Since we only look at the index finger and the middle finger in this work, it is unneccessary to perform time-consuming calculations for the other fingers. Three fingers were therefore removed from the model, the thumb, the ring finger and the little finger. The model then becomes simpler with fewer states and outputs and the calculations will be performed faster.

2.2 Experiment

To determine the accuracy of the methods an experiment was conducted. Markers were placed on each segment of the hand of a test subject and on a horizontal plate. More specifically, reflective markers, half-spheres of $2mm$ diameter, were attached using double-sided tape on the dorsal side of each joint of each finger. Three markers were also attached to the dorsal side of the palm, one on the ulnar styloid, one on the radial styloid, and one directly proximal to this along the radius. A photoelectric motion capture system (Oqus, Qualisys AB, Gothenburg) consisting of 8 cameras was used to track the 3D position of the markers in a measurement volume approximately $1m^3$. The frame rate of the system was 250 fps.

The test subject was asked to draw an eight with the index finger and the middle finger on the plate. When the finger is on the plate the z-coordinate of the finger tip is the same as that of the plate. All deviation from this value in the simulated z-coordinate must therefore be due to model uncertainty.

The mean square error between the z-coordinate of the finger tip and that of the plate is thus one possible measure of model accuracy. One way to check if the model succeeded with the noise reduction is to compare the variance of the modelled position of the marker with the variance of the measured position of the marker, during the time in which the finger is on the plate. To calculate the variance from measured data, we use the sample variance formula

$$v = \frac{1}{N-1}\sum_{i=1}^{N}(y_i - \bar{y})^2 \tag{2.10}$$

where $y_i, i = 1, \ldots, N$ are the measured data points, n is the number of samples and $\bar{y}$ is the sample mean

$$\bar{y} = \frac{1}{N}\sum_{i=1}^{N} y(i). \tag{2.11}$$

Figure 2.2 shows the z-coordinate of the finger nail marker and the z-coordinate of the plate. We see that there is a distance between the plate and the marker of about 0.6 cm. This is because the marker is on the finger nail and not on the finger tip in contact with the plate. There is also variation in the z-coordinate of the marker when the finger is on the plate, mostly due to measurement noise and small movement of the finger. By using the methods in section 2.1.1 and 2.1.2 we wish to reduce the variance and mean square distance to the plate.

2.2.1 Finding the finger tip

The markers on the distal phalanges of the index and middle fingers are on the nails and not on the finger tips. This means that the coordinates of the finger tips are not measured and are not generated by the model. They must be derived by using the models and their outputs. Since Method A and Method B use different models, the way to obtain the coordinates of the finger tips depends on the method used.

In Method A, starting from the origin of the root segment in the tree in figure 2.1 and performing all the transformations up to the distal phalange

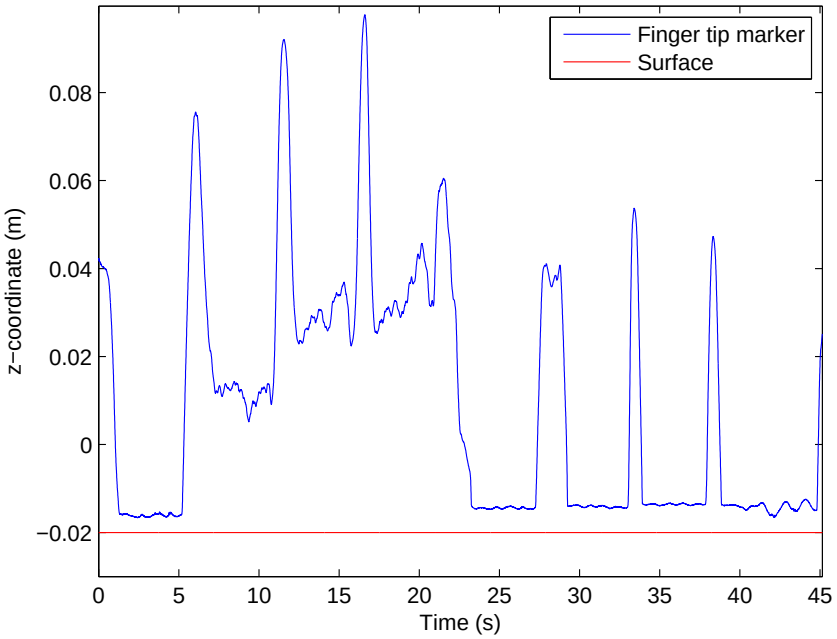

Figure 2.2: The z-coordinate of the measured position of the marker and the z-coordinate of the plate.

segment gives the coordinates of the segment origin. This is a point in the center of the finger where the distal phalange starts. The finger tip coordinates can be acquired by moving an appropriate distance along the segment's main axis. In order to do this, the orientation of the segment must be known at all times. The orientation is obtained by combining the rotation transformations between the root segment and the distal phalange segment in the tree in figure 2.1. These calculations involve lots of matrix multiplications and are not included here.

One of the outputs of the model in Method B gives the coordinates for the centre of mass of the distal phalange. To obtain the coordinates of the tip of the finger in this case, the same approach as in Method A can be used, but adding a distance to the centre of mass instead of the origin of the last finger segment.

Matematically, the way of finding the finger tip can be written as follows.

Assume $\mathbf{x}_0$ are the coordinates of a point in the middle of the finger. Assume that the tip of the finger is at a distance d along the axis given by the vector $\mathbf{v}$. The coordinates $\mathbf{x}_t$ for the finger tip is then obtained by

$$\mathbf{x}_t = \mathbf{x}_0 + d\mathbf{v}. \tag{2.12}$$

2.2.2 User Parameters

In both methods there are different user parameters which have to be set in advance.

In Method A the process noise σ_j^2 in (2.1) and the measurement noise $\mathbf{R}_\mu$ in (2.3) have to be specified. Large process noise for a state variable means that you think that the variation is large in that state, which means you have less trust in the model. The toolbox in Method A lets you specify one single parameter, which is then used to calculate σ_j^2 of each state in the model. The unit of each element in the process noise vector varies depending on its corresponding state. So it can be either m/s or rad/s, since states can be rotations and translations. The user parameter is unitless.

Since lengths of segments are estimated in this method it could be important to have accurate initial guesses for them. The initial values can be calculated in different ways. Since each segment has a marker and the markers are placed approximately in the middle of each segment, the lengths of the segments can be estimated by using the measured mean distance between the markers over time, during an experiment.

In Method B the lengths of the segments are not needed to specify the model. The parameters $\mathbf{R}_w$ and $\mathbf{R}_e$ in (2.5) and (2.9) must be chosen. $\mathbf{R}_w$ is calculated in the program code by using a tuning parameter ω. This parameter is used to decide the bandwidth of a filter that filters the process noise in the model. The larger the parameter the higher the bandwidth in the filter which results in larger noise. The parameter itself has no unit.

$\mathbf{R}_\mu$ and $\mathbf{R}_e$ are guesses of how large the measurement noise in the sensors are, and was already set in the program code of each method.

It is not possible to know in advance which the best parameters are. Different parameters must be tested and the results must be evaluated to find out which set of parameters gives the best results.

Chapter 3

Results

Both methods were run with different values of the user parameters and the mean square error between both the index finger tip and the middle finger tip and the plate were calculated for each case. The positions of the finger tips were calculated using the model output and the method in section 2.2.1. The results are shown below. The variance of the modelled z-coordinate of the finger nail marker was also calculated for each case.

3.1 Method A

The method was applied to the measured data using three different values of the user parameter deciding the process noises and two sets of initial values for the segment lengths. The user parameter was 5, 50 and 200. At first, all the initial values for the segment lengths and the distance between the knuckles were set to zero and were then changed to the values given by table 3.1. These values were calculated in the way described in section 2.2.2. The initial values of all other states were set to zero.

Figures 3.1 and 3.2 show the modelled z-coordinate of the index finger tip and and the middle finger tip respectively and the z-coordinate of the plate when the process noise parameter ρ was 50 and the initial values were zero, during the time in which the finger was on the plate. It can be seen that the position of the finger tip is not well estimated by the method in this case since there seems to be a distance of about 1.8 cm between the estimated

State description	State number	Initial value (cm)
Length of intermediate phalange of the index finger	15	3.24
Length of proximal phalange of the index finger	17	4.94
Length of intermediate phalange of the middle finger	22	3.77
Length of proximal phalange of the middle finger	24	5.63
Distance between knuckles	19	3.10

Table 3.1: Initial values for the segment lengths and the distance between the knuckles, and their corresponding state number in the model. Calculated in the way described in 2.2.2

index finger tip position and the real one, and 1.5 cm between the estimated middle finger tip position and the real one.

Figures 3.3 and 3.4 show the modelled z-coordinate of the index finger tip and the middle finger tip respectively and the z-coordinate of the plate when the process noise parameter ρ was 5 and the initial values were as in table 3.1, during the time in which the finger was on the plate. We see that this estimation is also poor, but better than in the case without initial guesses. The distance between the estimated index finger tip position and the real one is around 0.4 cm and the one between the estimated middle finger tip position and the real one is around 0.2 cm.

Figures 3.5 and 3.6 show the modelled z-coordinate of the index finger tip and the middle finger tip respectively and the z-coordinate of the plate when the process noise parameter ρ was 50 and the initial values were as in table 3.1, during the time in which the finger was on the plate. In this case the estimation is better since the z-coordinate of the finger tip seems to be close to that of the plate. We can also see that the variance of the modelled finger tip position is lower here.

Figures 3.7 and 3.8 show the modelled z-coordinate of the index finger tip and the middle finger tip respectively and the z-coordinate of the plate when

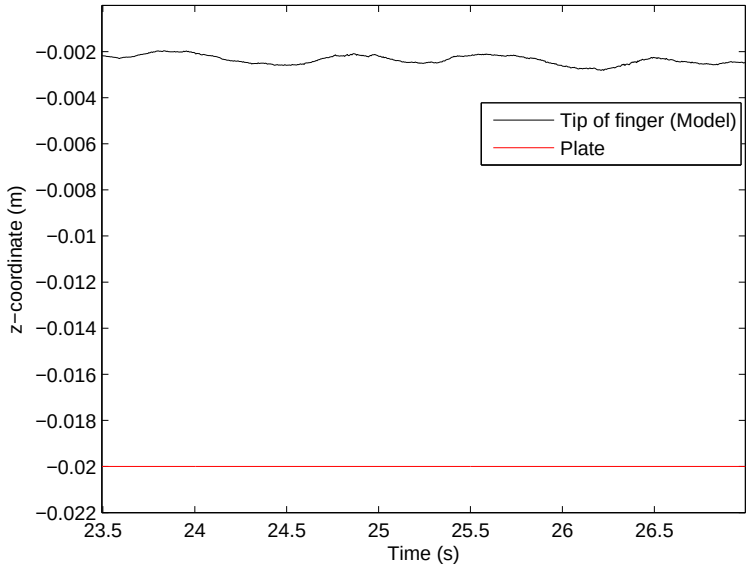

Figure 3.1: The modelled z-coordinate of the index finger tip and the z-coordinate of the plate using Method A with $\rho = 50$ and all initial values of the states zero.

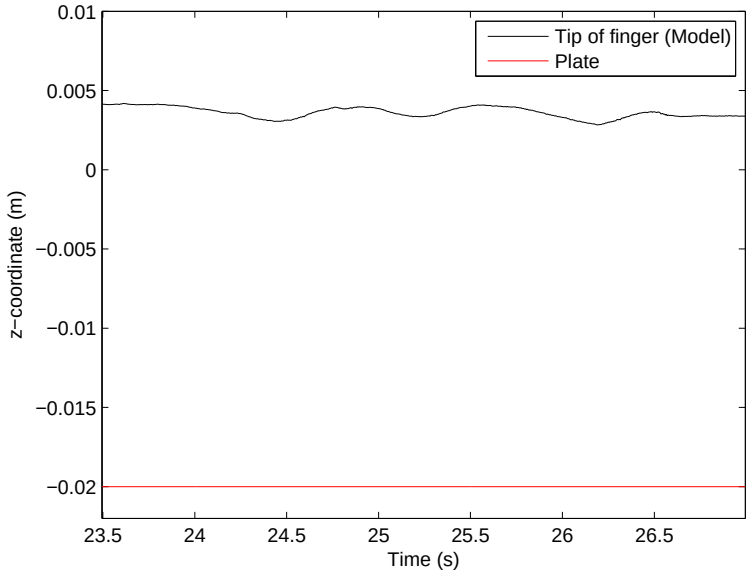

Figure 3.2: The modelled z-coordinate of the middle finger tip and the z-coordinate of the plate using Method A with $\rho = 50$ and all initial values of the states zero.

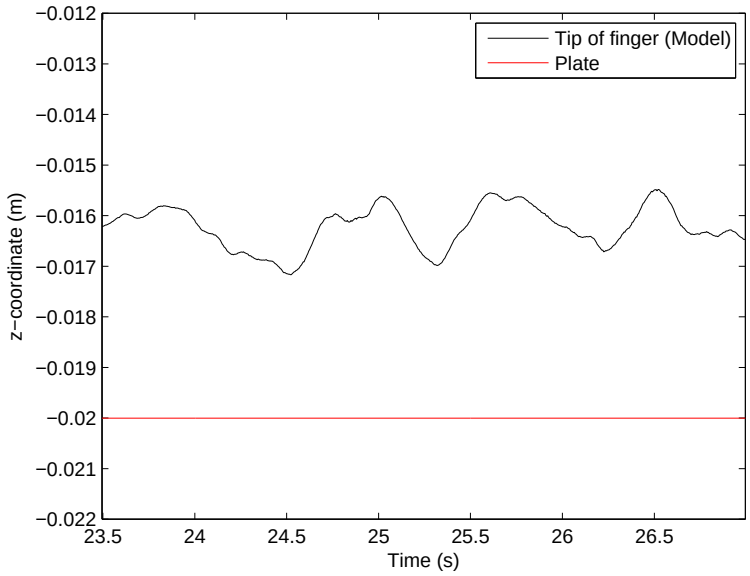

Figure 3.3: The modelled z-coordinate of the index finger tip and the z-coordinate of the plate using Method A with $\rho = 5$ and with initial values of the states as in table 3.1.

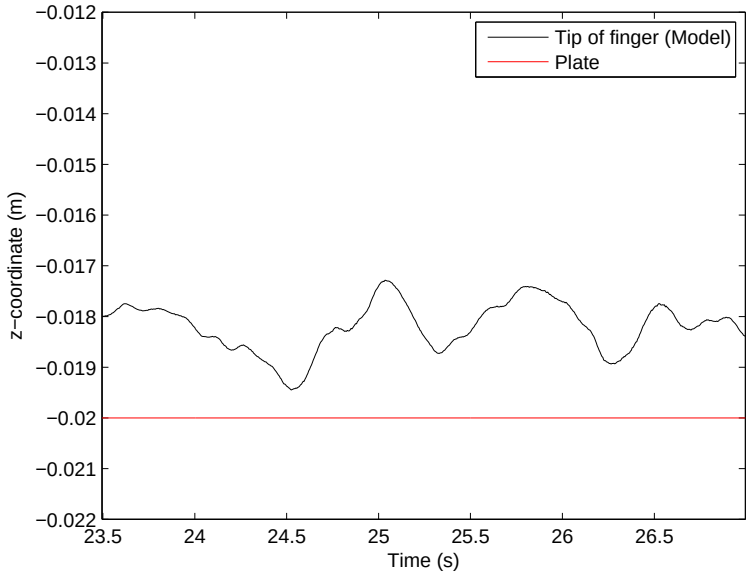

Figure 3.4: The modelled z-coordinate of the middle finger tip and the z-coordinate of the plate using Method A with $\rho = 5$ and with initial values of the states as in table 3.1.

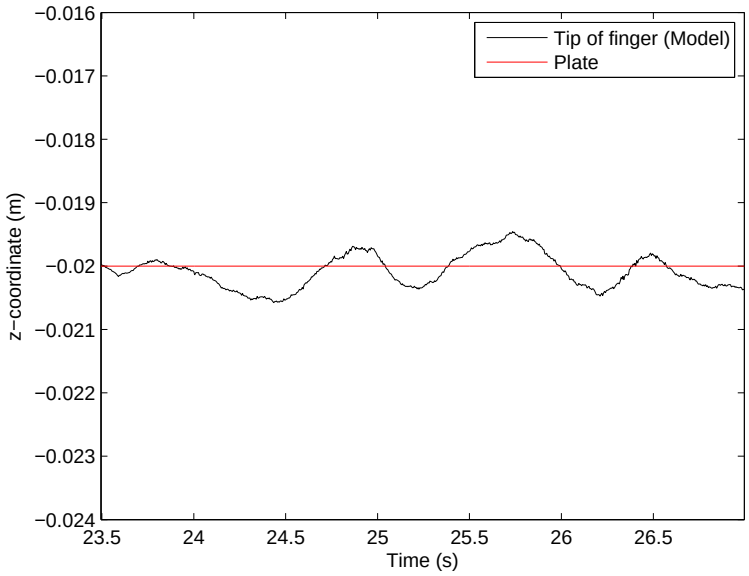

Figure 3.5: The modelled z-coordinate of the index finger tip and the z-coordinate of the plate using Method A with $\rho = 50$ and with initial values of the states as in table 3.1.

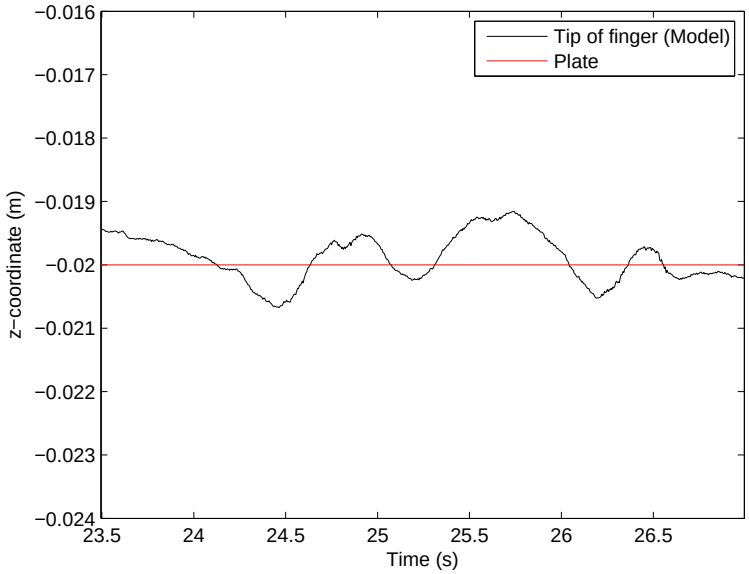

Figure 3.6: The modelled z-coordinate of the middle finger tip and the z-coordinate of the plate using Method A with $\rho = 50$ and with initial values of the states as in table 3.1.

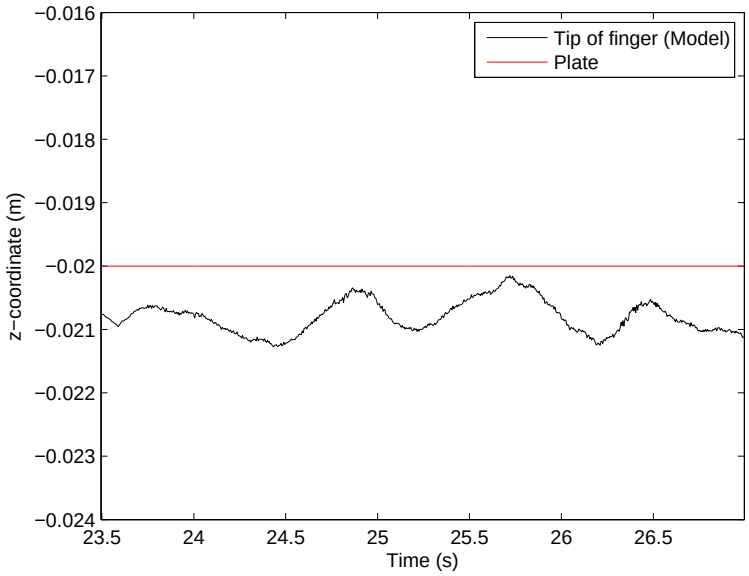

Figure 3.7: The modelled z-coordinate of the index finger tip and the z-coordinate of the plate using Method A with $\rho = 200$ and with initial values of the states as in table 3.1.

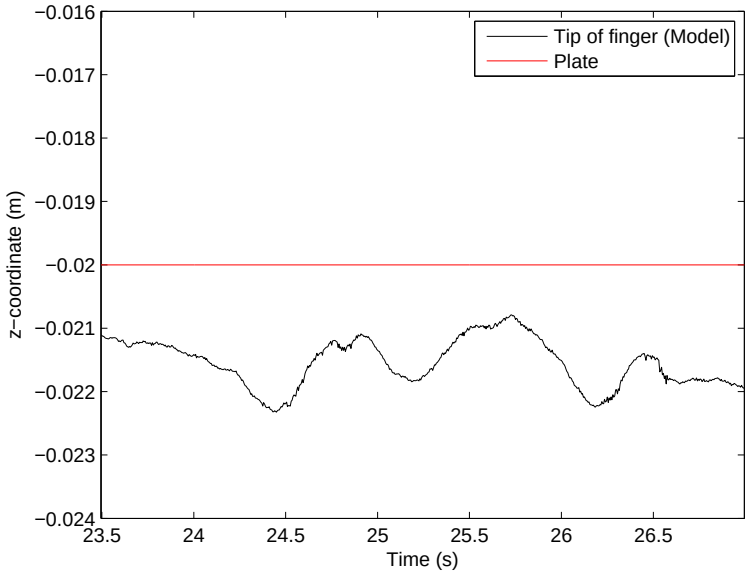

Figure 3.8: The modelled z-coordinate of the middle finger tip and the z-coordinate of the plate using Method A with $\rho = 200$ and with initial values of the states as in table 3.1.

the process noise parameter ρ was 200 and the initial values were as in table 3.1, during the time in which the finger was on the plate. This estimation is worse than the one shown in figure 3.5 but better than the estimation in 3.3. For each choice of the process noise parameter ρ and initial values the mean square error was calculated between the modelled z-coordinate of the finger tip and the z-coordinate of the plate. The variance of the modelled z-coordinate of the finger tip marker was also calculated.

3.2 Method B

The method was applied to the measured data using three different filter parameters, $\omega = 0.02$, $\omega = 1$ and $\omega = 100$. Figures 3.9 and 3.10 show the modelled z-coordinate of the index finger tip and the middle finger tip respectively and the z-coordinate of the plate when the filter parameter ω was 0.02, during the time in which the finger was on the plate. Figures 3.11 and 3.12 show the modelled z-coordinate of the index finger tip and the middle finger tip respectively and the z-coordinate of the plate when the filter parameter ω was 1, during the time in which the finger was on the plate. Figures 3.13 and 3.14 show the modelled z-coordinate of the index finger tip and the middle finger tip respectively and the z-coordinate of the plate when the filter parameter ω was 100, during the time in which the finger was on the plate. In all three cases the estimated finger tip z-coordinates are close to that of the plate, but when the filter parameter $\omega = 1$ the variance is smaller than in the other two cases. The variance is the largest when $\omega = 0.02$.

3.3 Performance

To compare the accuracy of the two methods the mean square error between the model z-coordinate of the finger tips and that of the plate in each case for each method was calculated. To check whether the methods succeeded in reducing the measurement noise, the variance of the modelled z-coordinate of the finger nail marker on each finger was calculated and compared to that

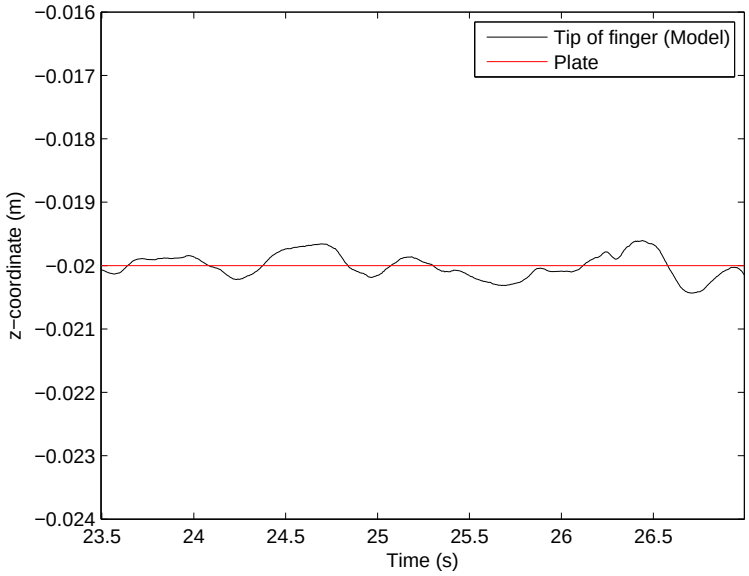

Figure 3.9: The modelled z-coordinate of the index finger tip and the z-coordinate of the plate using Method B with $\omega = 0.02$.

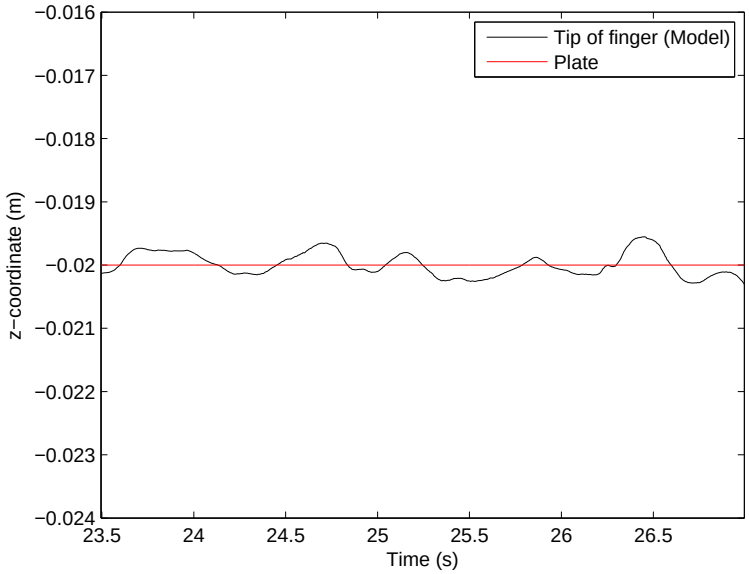

Figure 3.10: The modelled z-coordinate of the middle finger tip and the z-coordinate of the plate using Method B with $\omega = 0.02$.

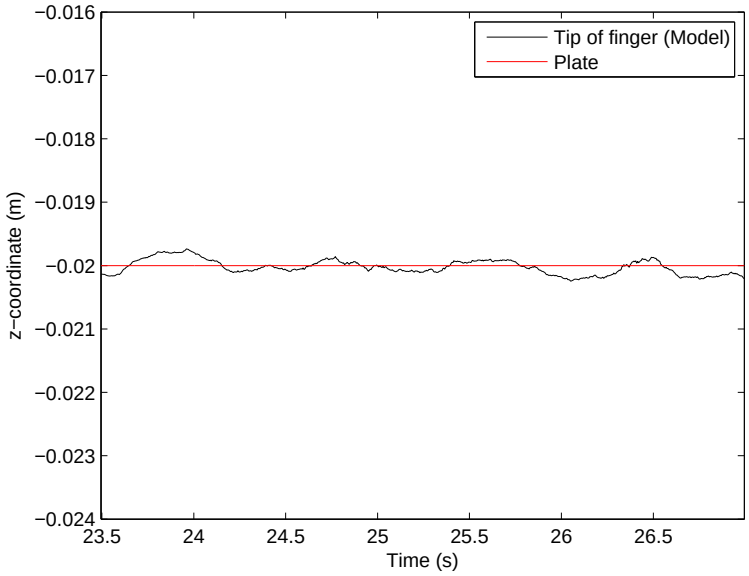

Figure 3.11: The modelled z-coordinate of the index finger tip and the z-coordinate of the plate using Method B with $\omega = 1$.

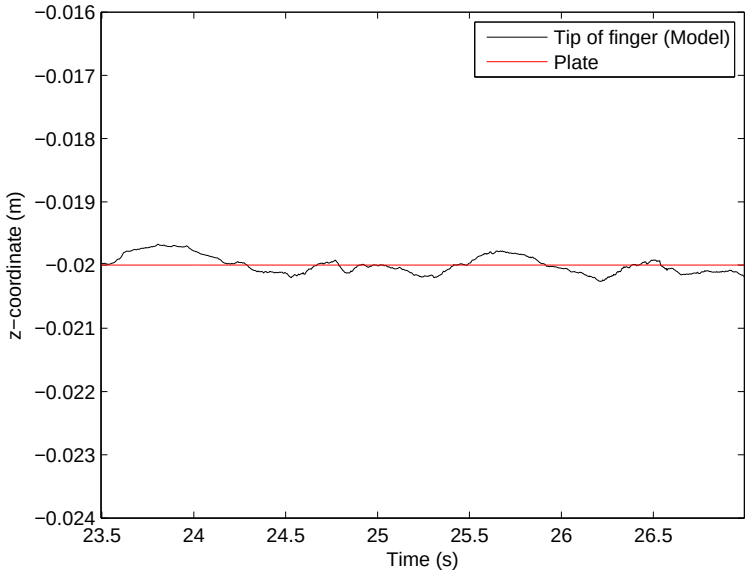

Figure 3.12: The modelled z-coordinate of the middle finger tip and the z-coordinate of the plate using Method B with $\omega = 1$.

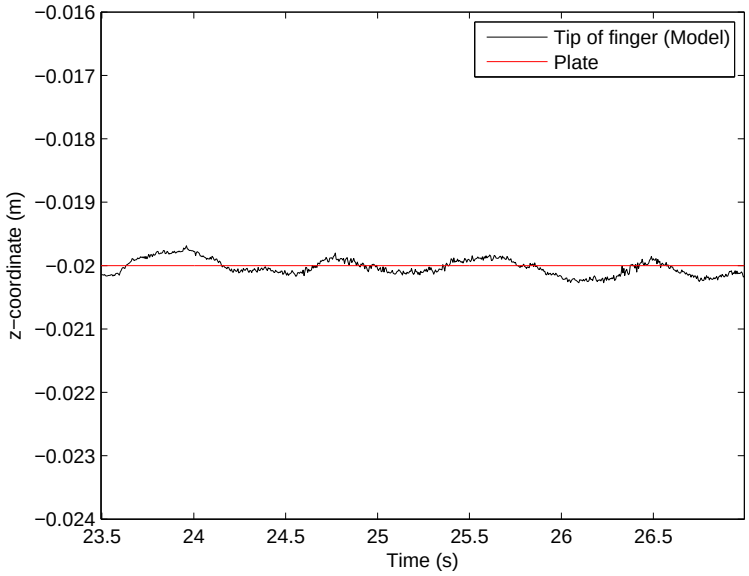

Figure 3.13: The modelled z-coordinate of the index finger tip and the z-coordinate of the plate using Method B with $\omega = 100$.

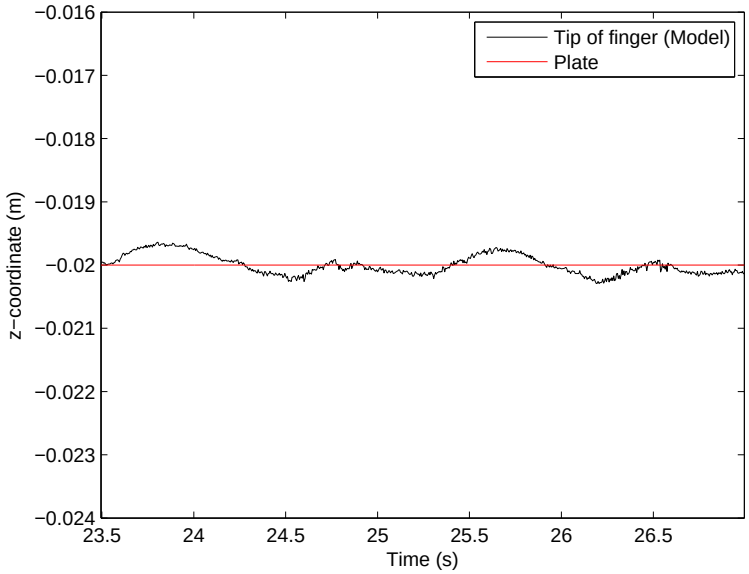

Figure 3.14: The modelled z-coordinate of the middle finger tip and the z-coordinate of the plate using Method B with $\omega = 100$.

of the measured z-coordinate. These values are shown in tables 3.2 and 3.3. The variance of the measured z-coordinate of the index finger was $3.74 \cdot 10^{-8}$ and of the middle finger was $5.48 \cdot 10^{-8}$. These variances were calculated using the sample variance formula in (2.10).

In Method A the mean square error was the smallest when using better initial values for the states and with $\rho = 50$. Changing the initial states increases the mean square error significantly, and so does changing the process noise parameter ρ. The variances of the *estimated* marker positions obtained from the model, were smaller than those obtained from the *measured* data, in all cases except for when the process noise parameter ρ was 5.

In Method B the mean square error was the smallest when ω was 1. Changing the filter parameter increased the mean square error, but not as much as when changing the process noise parameter ρ in Method A. In this case the variances of the *estimated* marker positions obtained from the model were smaller than those obtained from the *measured* data, in all cases except for when ω was 0.02 in the index finger case.

Finger	**Initial states**	**process noise parameter ρ**	**Mean Square Error (m)**	**Marker variance (m^2)**
Index	All zero	50	0.22	$3.56 \cdot 10^{-8}$
Index	As in table 3.1	5	0.01	$7.81 \cdot 10^{-8}$
Index	As in table 3.1	50	$5.64 \cdot 10^{-5}$	$2.37 \cdot 10^{-8}$
Index	As in table 3.1	200	$4.95 \cdot 10^{-4}$	$2.61 \cdot 10^{-8}$
Middle	All zero	50	0.39	$4.35 \cdot 10^{-8}$
Middle	As in table 3.1	5	$2.50 \cdot 10^{-3}$	$1.22 \cdot 10^{-7}$
Middle	As in table 3.1	50	$1.06 \cdot 10^{-4}$	$2.63 \cdot 10^{-8}$
Middle	As in table 3.1	200	$1.80 \cdot 10^{-3}$	$2.51 \cdot 10^{-8}$

Table 3.2: The mean square errors between the modelled z-coordinate of the index and middle finger tip respectively and that of the plate for different initial values and values of the process noise parameter ρ in Method A. The variance of the modelled z-coordinate of the finger nail marker is also included. The variance of the measured z-coordinate of the index finger was $3.7443 \cdot 10^{-8}$ and of the middle finger was $5.4801 \cdot 10^{-8}$.

Finger	**Filter Bandwidth**	**Mean Square Error (m)**	**Marker variance (m^2)**
Index	0.02	$2.67 \cdot 10^{-5}$	$5.42 \cdot 10^{-8}$
Index	1	$1.00 \cdot 10^{-5}$	$3.20 \cdot 10^{-8}$
Index	100	$1.2 \cdot 10^{-5}$	$3.63 \cdot 10^{-8}$
Middle	0.02	$2.48 \cdot 10^{-5}$	$5.21 \cdot 10^{-8}$
Middle	1	$1.42 \cdot 10^{-5}$	$4.28 \cdot 10^{-8}$
Middle	100	$1.74 \cdot 10^{-5}$	$4.89 \cdot 10^{-8}$

Table 3.3: The mean square errors between the modelled z-coordinate of the index and middle finger tip respectively and that of the plate for different filter parameters in Method B. The variance of the modelled z-coordinate of the finger nail marker is also included. The variance of the measured z-coordinate of the index finger was $3.7443 \cdot 10^{-8}$ and of the middle finger was $5.4801 \cdot 10^{-8}$.

Chapter 4

Conclusions and Discussion

4.1 Results

In table 3.2 and 3.3 we see that, based on the mean square error, Method B performs significantly better than Method A. All values of the mean square error in Method B are lower than the corresponding values in Method A. However, the mean square error in Method A, when the process noise parameter $\rho = 50$, is of the same order of magnitude as the mean square error in Method B, which means that as long as the choice of process noise parameter in Method A is good, it will perform almost as good as Method B. If we instead look at the variance of the modelled z-coordinate of the marker on the finger nail, it is about the same size for both methods. This indicates that both methods are equally good at reducing noise, but since we just saw that Method B performs better in terms of mean square error, the variance is not a good enough measure for determining which method works the best. Both methods succeed in lowering the variance of the position of the marker (for a good choice of process noise parameter/filter parameter) in comparison to the measured data, which indicates that the methods eliminates some of the noise.

The results of Method A depend a lot on both the choice of the process noise parameter and the initial guesses for the states, as can be seen in figures 3.1-3.8 and table 3.2. Choosing the wrong process noise parameter gives more

variance in the modelled z-coordinate of the finger tip, which means that the noise reduction is not as good. We can also see in figures 3.3, 3.4 and figure 3.7, 3.8 that the estimation of the position of the tip of the finger is incorrect if the wrong process noise parameter is chosen. When changing the process noise parameter from 50 to 5 the mean square error gets approximately 20 times larger, and when changing it from 50 to 200 it gets about 10 times larger. This is a problem since the exact process noise in the system is rarely known, and it is not always possible to guess an accurate value for it. In our experiment we knew that the finger tip was on a plate, which we knew the z-coordinate of and we could therefore use that as a reference. Choosing a poor initial guess gives an inaccurate estimation of the finger tip position, which is clear in figure 3.1. This is not desirable since it is not always possible to find reasonable initial values for the states.

In Method B, the accuracy of the estimation depends on the filter parameter. This can be seen in the mean square errors in the tables and the figures of chapter 3, but the effect on the estimation is not as large here as in Method A. Changing the filter parameter from 1 to 0.02 increases the mean square error with a factor of 2.67 and changing the bandwidth from 1 to 100 only increases it by a factor of 1.2. The expected value of the z-coordinate of the finger tip, when using Method B, seems to be the same as that of the plate, but the variance increases if a bad filter parameter is chosen. Method B should therefore according to these results always be preferred. The advantages of using Method A is that it was built with a toolbox that is easy to use and to adapt for other experiments and systems.

We see in figures 3.1-3.14 and in tables 3.2 and 3.3 that there are no large differences in the accuracy of the estimation between the index and middle finger.

4.2 Initial Guesses

We used the method in section 2.2.2 to find initial guesses of the states representing constant parameters. In this method the distances between markers

on connected segments are first obtained based on measured data. These distances are then used as estimates of the segment lengths. Another way to get the segment lengths, which could probably give even better guesses, is to physically measure the segments. Doing this was not a possibility, because it was not known until after the experiment was conducted that the initial guesses were going to be of importance. In the method of section 2.2.2, the result depends on where on the segments the markers are placed. The method is accurate if the markers are placed in the beginning of each segment (so the distance between two markers will be the length of a segment) but in fact they are put somewhere in the middle of each segment, which will make the distance between them vary as the fingers bend.

4.3 Position of the Finger Tip

The coordinates of the finger tip can not explicitly be obtained from the models, instead it has to be calculated. The method in section 2.2.1 requires knowledge of the distance between the origin of the distal phalange to its finger tip in Method A, and from the segment center of mass to the finger tip in Method B. These distances must be estimated or measured. The method in section 2.2.2 can not be used to estimate these lengths since there is only one marker placed on the distal phalange. In this work the lengths were measured manually on a different person than the test subject used in the experiment. This can have contributed to incorrect mean square error values. Another problem with using the method in section 2.2.2 is that it assumes that the distance from the origin/center of mass of the distal phalange to the finger tip is constant, but that is not necessarily the case since the finger is soft and is deformed if pressed hard against the plate.

4.4 The Accuracy Measure

Using the mean square error between the estimated finger tip position and the plate, is the accuracy measure used in this work. This is a natural measure to

use when the goal is to estimate the positions of the finger tips as accuratly as possible while they are moving over a plate, but it does not say a lot about how good the methods are at estimating the position for other parts of the system. It also does not say how good the methods are at estimating the finger tip positions in experiments where they are not on a plate, but perhaps moving freely in the room.

4.5 Future Studies

There are a lot of things that can be studied in more detail. In this work the accuracy of the methods was only evaluated when the fingers were moving over a flat surface. It can also be of importance to know the performance of the methods when the fingers are moving in other ways. To be able to evaluate that, other experiments has to be conducted and other accuracy measures must be used. For example, the test subject could move the finger tips over a known surface that is not flat, and the mean square error between the finger tips and that surface could be calculated.

In this work only the estimation of the positions of the finger tips was evaluated. Determining the position of other parts of the hand can also be important, and the accuracy for such methods should also be investigated.

The models could be simplified further by only modelling one finger instead of two. We chose modelling of both fingers to see if there were large differences between the estimations of the positions of the index finger tip and the middle finger tip, but since the experiments showed that the difference is small, additional simplifications could be done.

Bibliography

[1] T. B. Moeslund and E. Granum *A Survey of Computer Vision-Based Human Motion Capture* Computer Vision and Image Understanding, Vol. 81, 2001.

[2] P. Olsson, S. Johansson, F. Nysjö, and I. Carlbom *Rendering Stiffness with a Prototype Haptic Glove Actuated by an Integrated Piezoelectric Motor* Conference paper, Euro Haptics, 2012.

[3] E. Todorov *Probalistic inference of multi-joint movements, skeletal parameters and marker attachments from diverse motion capture data* IEEE Transactions on biomedical engineering, Vol. 54, 2007.

[4] K. Halvorsen, C. Johnston, W. Back, V. Stokes and H. Lanshammar *Tracking the Motion of Hidden Segments Using Kinematic Constraints and Kalman Filtering* Journal of Biomechanical Engineering, Vol. 130, 2008.

List of Figures